eprints@whiterose.ac.uk
https://eprints.whiterose.ac.uk/

Development of metacage for noise control and natural ventilation in a window system

Gioia Fusaro[1,2], Xiang Yu[1], Jian Kang[3†] and Fangsen Cui[1†]
[1]Institute of High Performance Computing, A*Star, Singapore
[2]Acoustics Group, School of Architecture, University of Sheffield, UK
[3]Institute for Environmental Design and Engineering (IEDE), The Bartlett, University College London, UK
[†]Corresponding author: cuifs@ihpc.a-star.edu.sg

Abstract

Ventilation window is one of the critical elements in sustainable building development, although frequently, outdoor factors such as environmental noise can limit their use. It is necessary to develop windows with both natural ventilation and noise mitigation functions. Acoustic Metamaterials (AMMs) set a new trend in solving physical challenges related to sound wave control, which can find their applications in ventilation window. This study presents a design based on acoustic metacage concept to enhance the window's natural ventilation and acoustic performance. Finite Element Method (FEM) is used to study and optimise the acoustic performance of the metacage window. The ventilation is evaluated at the same time following predefined guidelines related to the window's opening ratio and air-flow directivity. The metacage window structure finally, reduces the noise transmission with a mean value of 30 dB within a frequency range of 350-5000 Hz and has an opening ratio of the 33% compared to the whole system surface. The front panel gives a mean high frequencies TL contribution of 17 dB (2000-5000 Hz). Additional lateral constraint and cavities increase the TL performance up to 70% on a wider lower frequency range (350-5000 Hz). Thanks to the cavities, the resonant unit cells among the acoustic metasurface (AMS) significantly suppress sound from exiting the structure in broadband frequencies and allow bigger opening on the lateral side. This significantly contributes to the natural ventilation potential of the metacage window, which in the long term, becomes equally effective to the conventional open windows.

1. Introduction

Natural ventilation is an energy-efficient approach. [1], [2] People in modern times spend over 70% of their day indoors, which emphasizes the importance of a comfortable indoor environment. [3], [4] However, indoor comfort through natural ventilation is frequently limited by outdoor inputs, such as noise sources. Different noise mitigation windows can reflect or absorb the incident acoustic energy. Active noise control can be used to create low-frequency stopbands. [5], [6] Rolling shutter boxes are shown to be a reasonable noise control passive system. [7] For both active and passive systems, an increased thickness is usually needed to obtain a wideband attenuation in the frequency range between 350 and 5000 Hz. [8], [9] These methods do not guarantee the required airflow, precluding their usage in applications where ventilation is required.

Thanks to the development of acoustic metamaterials (AMMs), a brand new diversity of manipulating the sound wave have come up. The subwavelength structure of metamaterials determines more effective acoustic properties according to their structural shape rather than their constitutive materials. Acoustic metamaterials for wave-front modulation [10], [11], sub-diffraction imaging [12], and acoustic cloaking [13] have been demonstrated and may be considered for building uses. [14], [15] In the mechanical engineering research area, acoustic metamaterials have inspired a series of acoustic ducts for noise reduction [16]–[20], the applicability of which may be extended in buildings structures. Their inherent large spatial footprint of duct limits their versatility and flexibility during implementation. For these reasons, improvements are needed to align ventilation and noise control targets to the buildings (and so windows) requirements in a broader range (350-5000 Hz).

Natural ventilation is generally meant to be performed according to three window parameters: the opening size (or opening ratio), the air-flow directivity, and the time addressed for the ventilation. [21], [22] For the first parameter, generally bigger opening induces larger air mass flow, higher air change rate (ACR) and CO_2 removal rate. [1] Secondly, the normal direction of the air-flow towards the window wall (horizontal pivot or turning window) has been proved to be the best solution for obtaining an efficient ACR in a short amount of time [2], [21], while lateral air-flow direction (such as in tilt or awning windows) requires a longer amount of time to reach the same ACR. Ventilation time as the final parameter determines the exposition of the indoor environment to the inputs (such as harmful noise) of the outdoor and vice-versa according to the window characteristics. By combining these parameters, it is possible to achieve window design for different indoor functions. In a perforated panel, for example, [17] sound waves and airflow are blocked according to the orifice size. Smaller perforated holes and perforation ratio will yield better sound insulation while poorer ventilation.

Although there are several previous works attempting ventilation and noise reduction through AMMs [16], [21], it is still rare to see the substantial potential for window application in a wide frequency range. For this reason, this study aims to 1) proving sound reduction and ventilation performances of a tunable AMM structure to be used for window design, and 2) investigating which are the determinant factors for such vital features. Following the sub-structuring approach of Yu et al. [23], and starting from the concept of AMM, ventilated unit cells with local resonant cavities are chosen to allow better ventilation and sound reduction, ideally offering high flexibility for geometric tuning and subsequent acoustic optimization. Through some preliminary analyses on the acoustic properties of the proposed unit cell, the geometry is fixed, and its sound attenuation in TL is characterized. Afterwards, an array of unit cells is analysed

as acoustic metasurface (AMS) which, folded into an octagonal shaped acoustic metacage [14] creates the AMM. Different geometrical configurations of the AMM are then compared in terms of TL and ACR to establish which is the optimal one.

2. Acoustic unit cell characterisation

2.1 Design of acoustic unit cell

The AMM window is based on a hierarchical geometry at the base of which, there is the unit cell. Considering the schematic in FIG. 1, which is composed of two symmetric resonant parts characterised by inclination α and several cavities decreasing in lengths along the z-axis and open towards a central duct. The tailoring of the inner structure creates local resonances in order to form a stop-band. The unit cell can be considered as a waveguide attached with periodic scatterers in the lateral direction for flow exit. This specific system is based on the theoretical wave propagation and the existence of stop-band related to both constant and linear structures such as the AMMs based on the resonant tubular array and the acoustic black hole (ABH). [24], [25]

Table 1: Geometric variables involved in the acoustic unit cell characterisation process

(α) Rotation angle	(n) Cavities Number							
	4	5	6	7	8	9	10	
	(a) Cavities Width							(b) Unit cell height
45°	0.016	0.013	0.011	0.009	0.008	0.007	0.006	0.066
55°	0.019	0.015	0.013	0.011	0.009	0.008	0.007	0.077
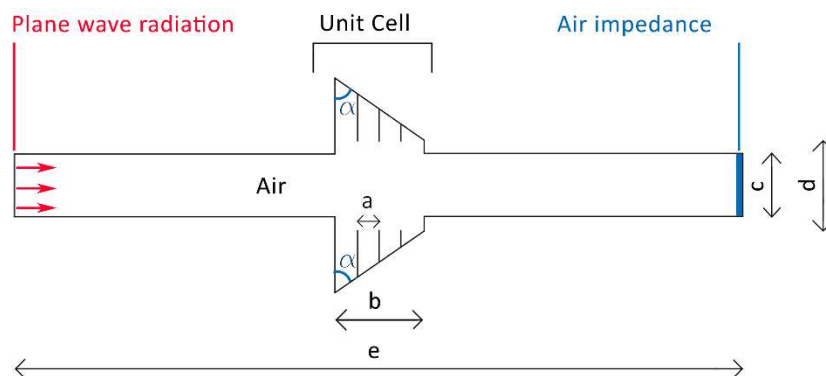
FIG. 1 Geometrical settings and boundary conditions for the particular of the acoustic unit cell with cavities width (a), tip height (b), tube width (c), smaller tip base (d), tube length (e), rotation angle (α).

In order to suppress sound wave, the resonators lined along the duct in a unit cell provide locally resonant stopbands, while exerting minimal airflow interruption. In Table 1 are shown the three parameters that define the structure and which are investigated: the inclination of the unit cell's lateral sides ('rotation angle'), number of cavities, and width of the cavities. The tube used for this parametric study has a length of 0.6 m and a width of 0.05 m (Table 1 and

FIG. 1). The smaller unit cell base ('d' in FIG. *1*) is 0.055 and 0.080 m when the rotation angle is respectively 45° (FIG. 2.a) and 55°(FIG. 2.b).

2.2 Numerical study on the acoustic unit cell

Two-dimensional simulations are carried out by COMSOL Multiphysics, Pressure Acoustics Module, in order to understand the TL characteristics of the unit cell. A plane wave incidence is applied to the left end of the 2D tube (incident pressure = 1 Pa), and the walls of the tube and resonant cavities are set as sound hard boundary. At the tube outlet, air impedance is given to allow sound wave exiting with no reflections. The mesh size is determined according to the FEM criterion, where at least six nodes are used to simulate a wavelength in air. The maximum allowable element size is 343/6/5000=0.0114 m, in order to reach 5000 Hz. The frequency domain analysis covers a frequency range from 350 Hz to 5000 Hz with a step size of 100 Hz. The frequency range between 350 and 5000 Hz is chosen to be a realistic approximation of the average environmental noise. [26] The averaged incoming sound power at the inlet boundary, and outgoing sound power at the outlet boundary are used to calculate the TL, following the equation $TL = 10 \log_{10}\left(\frac{w_{in}}{w_{out}}\right)$ [dB]. An increase in the TL curve will thus indicate less efficient sound transmission because sound energy is more confined in the cavities.

This methodology has been already proved several times by Yu et al. showing the effectiveness of such numerical prediction validated efficiently by experimental test. [16], [23] So it is reasonable to consider that, in this case, with similar boundary conditions and simulation settings, the numerical study is an efficient instrument for accurate acoustic performance prediction. Further experimental validation could improve the methodology but is not a fundamental part at this stage.
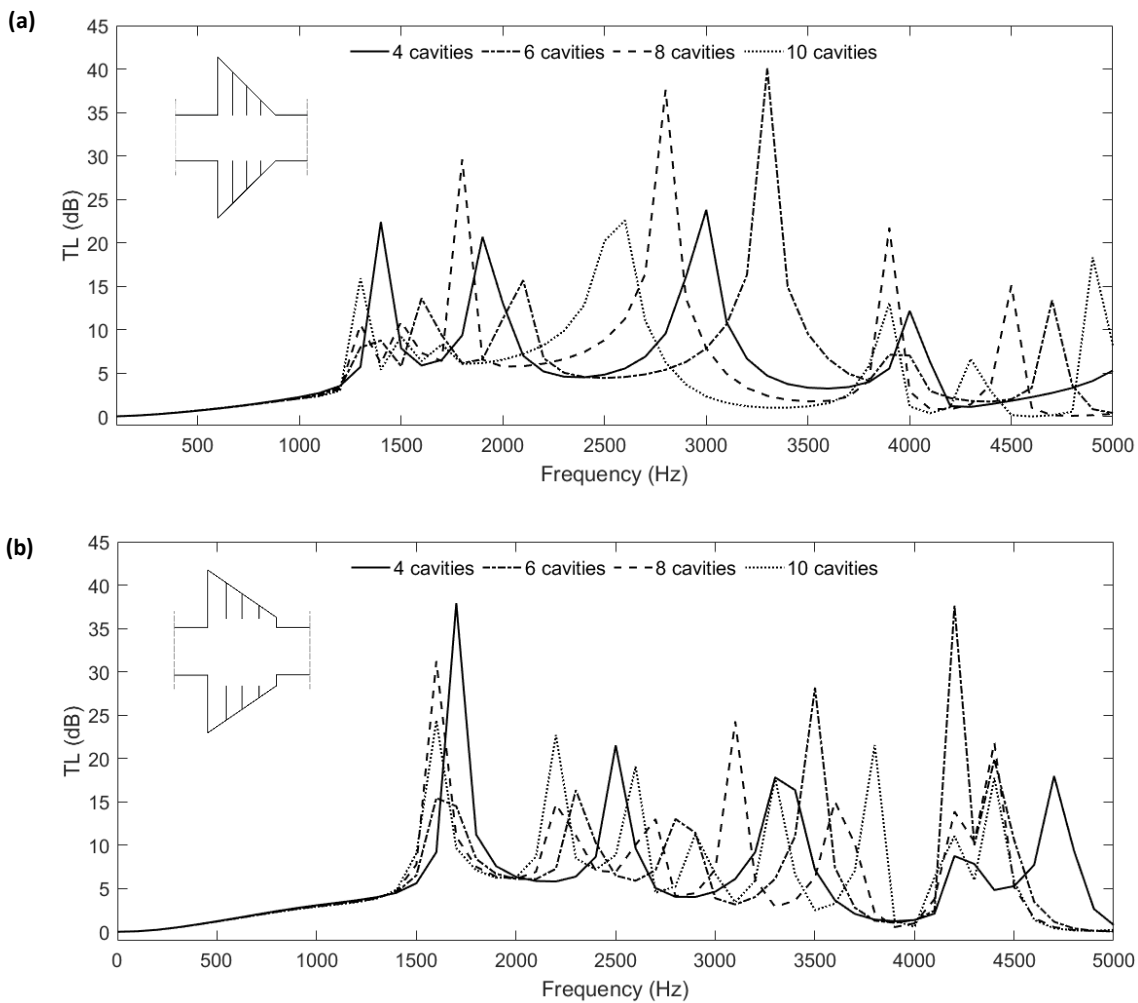
FIG. 2 Transmission Loss related to α= 45°(a), and α= 55° (b), for the sake of simplicity, only even numbers of the cavities parametrisation results, are shown.

The parametric study highlights interesting correlations between the cavities and the duct's width and the consecutive TL behaviour. For example, FIG. *2* shows the TL results for 4,6,8,10 cavities number combination. From these graphs, it is observed that as the inclination angle increases, the peaks are higher since the cavities are more prolonged, producing more substantial resonance effect. In this case, a broader average TL is achieved. At the same time, the TL peaks rise when the cavities number is less. Generally, the frequencies with effective sound attenuation are shown to be significantly affected by the resonator geometry.

This part of the study shows how the unit cell geometry is characterised and which parameters combination is best in terms of ventilation potential and noise reduction. So the system with the angle α= 55°, and n= 4 (see FIG. 2.b) is considered in the further numerical analysis, due to broad TL capacity combined with a wider central duct (so higher ACR potential).

3. Resonance-induced localised modes in the AMM: Physics principles behind the acoustic metacage window

FIG. *3*.a shows the transversal section of the developed metamaterial. The model has an axisymmetric configuration concerning the directions passing through the centre of the metacage window *o* with a pace of $k\pi/4$ with a transversal uniform thickness of *t* (x-direction). For the sake of simplicity, the use of a second axial reference such as *z'y'* is necessary to study the wave propagation in a radial reference system (see FIG. 3.b). In this reference system, *z'* is each direction passing through the centre *o* with a pace of $k\pi/4$, starting from the axis *z*, and *y'* is the perpendicular direction. The incoming pressure (P_{in}), the density (ρ_0), and the velocity in the medium (air) (c_0) are considered as uniform in the transversal section (FIG. 3.a). Therefore, a specific impedance and refractive index can be assigned to the different geometrical areas of the metacage window. Region 1 (approximately *r< r1*, FIG. 3.b) is characterised with an acoustic impedance of Z_1 and refractive index of n_1 and region 2 (approximately *r1 <r <r2*) has an acoustic impedance of Z_2 and refractive index of n_2. Due to the contrast in refractive indices of the two regions, while the sound wave travels through towards the unit cell, in region 1 it remains in a continuum state (we assume the reflection on plane *xy* like a constant). On the contrary, when the sound waves travel through region 2, it interacts with the relative resonance-induced localised modes. After passed region 2, it will result in an out-of-phase condition. The incident acoustic wave travelling through the metacage window will enter region 2 having a small phase shift, with a consequent destructive interference on the transmission sides of the metamaterial unit cell (FIG. 3.b).
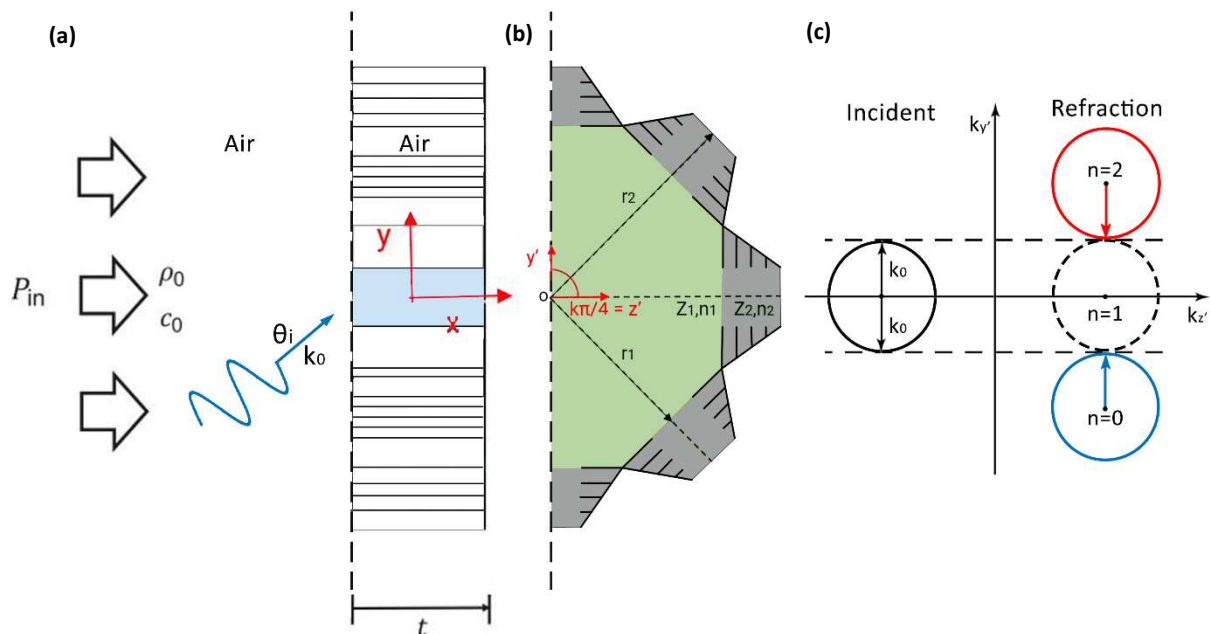
FIG. 3 Schematic of the physical characteristics according to the metacage window geometry: a)Transversal section of the whole structure (plane xy), b) particular of the frontal section of the AMM (plane zy), highlighting different gradient metamaterial grating with both sides of the AMM that are air, c) iso-frequency contours for ξ = G = $2k_0$.

In this case, the grating order should be considered as in the generalised Snell's law for metasurfaces.[27] The particular studied system is composed of one internal cavity with eight unit cells with four different cavities (sub-unit cells) in one period *p,* which in this case

---

correspond to r_1 and r_2. The relative wave with the angle of incidence θ_i and the refraction angle θ_t can be calculated using the generalised Snell's law [10]

$$(\sin \theta_t - \sin \theta_i)k_0 = \xi + nG \tag{1}$$

Here k_0 is the wavenumber in free space, $\xi = dF/d\,z' = 2\pi/p$ is the phase gradient along the surface (along the *z'*-direction in FIG. 3.b) on the right outgoing interface, *n* is the integer representing the order of diffraction (or grating order), and $G=2\pi/p$ is the reciprocal lattice vector (depending by the reciprocal lattice of the cavity and the unit cells). It is noted that only when the period is comparable with the wavelength λ the term *nG* appears [10], for large angles of incidence. Comparing the unit cell system with the supercell developed by Quian et al., the physics related to both can be studied through the example case of $p = \lambda/2$ by the assumption that the period is less than half the wavelength ($p \leq \lambda/2$).[28] Since in this case $\xi = G = 2\pi/p = 2\,k_0$, eq. (sin θt - sin θi)k0 = ξ + nG   (1)
can be rewritten as

$$\sin \theta_i = \sin \theta_t + 2(1+n) \tag{2}$$

The iso-frequency contours for $\xi = 2\,k_0$ in FIG. 3.c are employed to study the importance of different incident angles on the propagation character of the incident wave impinging on the unit cell (solid circle). As demonstrated by Quian et al., if $\xi = 0$, there are no phase shifts introduced along with the interface (black dashed circle in the refraction part of FIG. 3.c). Consequently, a black dashed circle displacement of $\xi = 2k_0$ appears when phase shifts are introduced along with the interface. So in FIG. 3.c the lower blue circle corresponds to $n = 0$ in eq. (2), while the red circle corresponds to $n = 2$ in eq. (2). Generally, the incident wave couples more easily with such two propagation orders ($n = 0, 2$) rather than higher ones. The incoming wave to couple into propagating modes has a critical angle expressed as $\theta_c = \sin^{-1}(1 - \xi/k_0)$ for 0th order diffraction (i.e., $n=0$). When the period p is a minimal value, i.e., $p < \lambda/2$, then $\xi = 2\pi/p > 2\,k_0$. For this reason, and since $|1 - \xi/k_0| > 1$, the critical angle θ_c becomes an imaginary number, meaning that the propagating mode for an arbitrary angle of incidence θ_i and $n=0$ is not allowed through the AMM. On the other side, for arbitrary non zero value of $n+1$ (*n* is an integer), the mode-coupling method can be used to interpret the transmission coefficients. [14] The nth-order diffracted wave (recalling that $\xi=2\pi/p$) has an *y* component of the wave vector defined by the equation $k_{y',n} = \sqrt{k_0^2 - \left[k_{z'} + \frac{2\pi(n+1)}{p}\right]^2}$, where $k_{x'}$ is the component of the wave vector on the *x* axis. Since $p < \lambda/2$ for an arbitrary non zero value of $n+1$, we shall have $\left|k_{z'} + \frac{2\pi(n+1)}{p}\right| > \frac{2\pi}{\lambda} = k_0$ (note that $|k_{z'}| < \frac{2\pi}{\lambda}$), meaning that $k_{y',n}$ becomes imaginary for any non-zero value of $n+1$. For this reason, the transmitted waves are evanescent and decay exponentially along the *z'* direction on the plane *z'y'*. Nevertheless, since $k_{y',n}\left(k_{z'} + \frac{2\pi(n+1)}{p}\right)$ is still a real number, it is essential to stress further that the propagation of surface waves in the *y'* direction is still possible. For *n=-1*, although the propagating waves are allowed, their transmission is minimal due to destructive interference [14]. In conclusion the transmission trough the AMM for $p < \lambda/2$ is small regardless of the angle of incidence for any value of *n*, and the AMM design can be used as an omnidirectional sound barrier for all-angle incoming waves.

4. Development of the metacage and the acoustic performance

4.1 Sub-structural design of the acoustic metacage window

As depicted in FIG. *4*, an array of 8 unit cells can be considered as an Acoustic Metasurface (AMS) [23], where identical unit cells with the same resonance and phase properties can allow homogenous sound isolation effect. The AMS can be folded into a ring shape to realise an acoustic metacage [14] to confine acoustic transmission in all directions. Based on the chosen unit cell geometry, 8 unit cells form an octagon-shaped metacage, which is applied to separate two acoustic domains, as shown in FIG. *4*.b. The domain with incoming waves is denoted as the "noisy" side, and the transmission side is denoted as "quiet". The octagonal opening of the metacage opens fully to the noisy side, allows air to enter with sound waves. The metacage front facing the quite side is closed with a rigid panel, which forces sound to exit through the eight lateral unit cells, thus interacting with the resonant cavities. Analytical and numerical analyses are performed, to investigate the system effectiveness according to each part contribution in terms of TL (configuration without the metacage window, configuration with only the front panel, configuration with lateral constraint, configuration with cavities). Finally, in the discussion, the ventilation capacity of the final model is compared with other ordinary window models to address the ventilation parameters mentioned above. The efficiency of the opening ratio combined with the noise reduction is analytically and numerically demonstrated, and a new technique for long term consistent ventilation and noise reduction on the middle-high frequency range (350-5000 Hz) is defined.
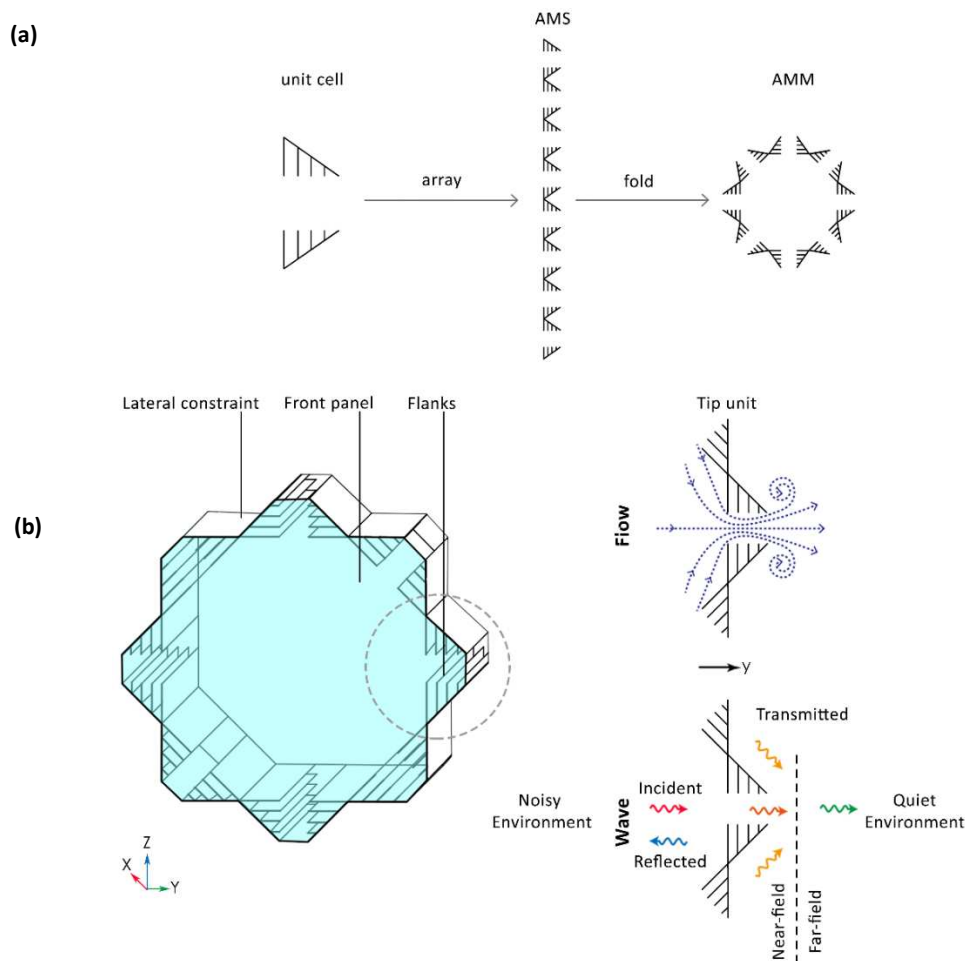
FIG. 4 Metacage window system: a) AMM geometrical concept and b) schematic of the flow and the wave propagation.

4.2 Numerical analysis: unit cell, AMS, and AMM

After the analytical analysis of the AMM structure, the 3D simulation is defined as semi-infinite acoustic conditions are applied to the spherical geometrical boundaries as depicted by FIG. *5*. The overall boundary sphere has a diameter of 0.7 m and is centred with the analysed geometry. The metacage window has a total height of 0.6 m (maximum distance between two opposite unit cell tips). The background pressure field is defined in the noisy side as incoming waves, while the entire semi-sphere surfaces are assigned with free wave radiation conditions (see FIG. *5*.b). The walls of the metacage and material cells are set as interior sound hard boundaries. Sound transmission through walls of the metacage and possible viscous-thermal effect in the narrow resonator channels are neglected in this study. The 3D domain is filled with air, where air density and sound speed at room temperature are used. TL is calculated by the reduction of sound power through the metamaterial interface (in decibel). Regarding the mesh size for the 3D study, this model results very complex and, since the convergence of results is proved, simplification is needed. So the maximum allowed element size is increased at $343/6/2500=0.0228$ m. In the results, the TL and SPL distribution are shown linearly and superficially within the simulation frequencies.
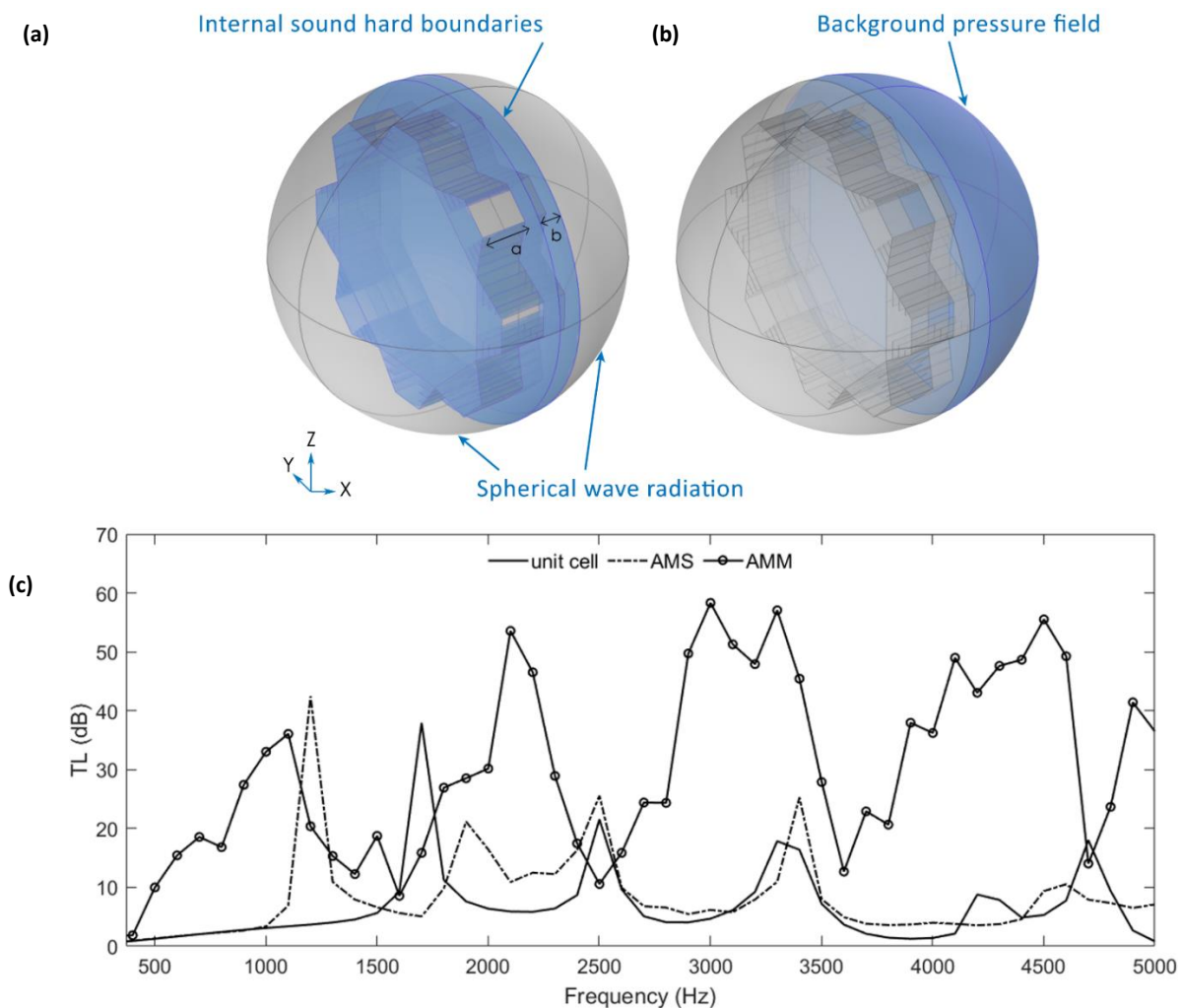
FIG. 5 3D boundary conditions in the FEM settings: a) internal sound hard boundary, b) background pressure field, where a=0.1 m, and b= 0.05 m; and c) TL results of the unit cell, AMS, and AMM for a frequency range of 0-5000 Hz expressed in dB.

Results of TL related to the unit cell, AMS and AMM are presented in FIG. *5*, where the array of 8 unit cells considered as a metasurface, is investigated with the same 2D physical boundary condition of the unit cell. The unit cell TL analysis shows peaks at 1700, 2500, 3300, and 4700 Hz (FIG. *5*). The AMS determines a higher TL in the lower frequencies with peaks at 1200, 1900, 2500, and 3400 Hz, and the mean value of ΔTL=2dB compared to the unit cell mean TL. Finally, by folding the AMS in a loop (generating the AMM), a broader increase of the TL is achieved (mean value of ΔTL=22dB compared to the AMS TL). This phenomenon is probably due to the three-dimensional configuration characterised by a front panel (FIG. *4*) that contributes to reflecting the sound wave backwards. This and other AMM configurations contribution need to be further investigated. The comparison between them can give insights into the sound attenuation mechanism and reveal the critical parts determining the effectiveness of the overall system.

4.3 Numerical analysis: different AMM configurations comparison.
As a comparison, four configurations are studied, as illustrated in FIG. *6*.a-d. The first configuration (FIG. *6*.a) includes only the opening between the two acoustic domains. The second configuration (FIG. *6*.b) inserts a rigid frontal panel, but sound can still exit freely from

the lateral side. The third configuration (FIG. *6*.c) includes the structure with nozzle shaped unit cells, but the resonant cavities are missing. This is quickly done by removing the interior flanks inside the unit cells. The last configuration (FIG. *6*.d) is the proposed 3D acoustic metacage window design. The TL curve in FIG. *6* shows that for Configuration 1, there is no significant TL. This is typically between 0-3 dB and sets a reference value for other configurations. Note that if the front and back panels of the metacage are both opened, the acoustic effect is similar despite the presence of any unit cell elements. For the other three configurations, the TL results in FIG. *6*.e show a dome-like behaviour, typically appearing in the TL pattern of expansion acoustic ducts. [19] Since the expansion ratio and unit cell volume characterized by the primary dimension is almost the same, the tendency of the slopes in the three configurations is similar, with peaks appearing near 1100, 2100, 3000, 3300, and 4500 Hz. The amplitude of TL is, however, different due to reasons to be discussed later. For example, as stated in the previous analytical considerations, the comparison between curve 1 and 2 in FIG. *6* shows the crucial importance of the front panel for sound reflection. As showed by FIG. *7*.a, when the acoustic wave interacts with this part of the metacage window, it is partially reflected back and partially passes through the lateral space between the front panel and the division towards the quiet environment. The barrier performance of the second configuration is only effective by cutting the direct "line of sight" between source and receiver. [29] The results also show that along with the common knowledge, high-frequency sounds are more incline to be attenuated by the front panel than low-frequency sounds due to their low wavelength. A longer wavelength sound will easily pass through the barrier by diffraction (FIG. *6*.e).
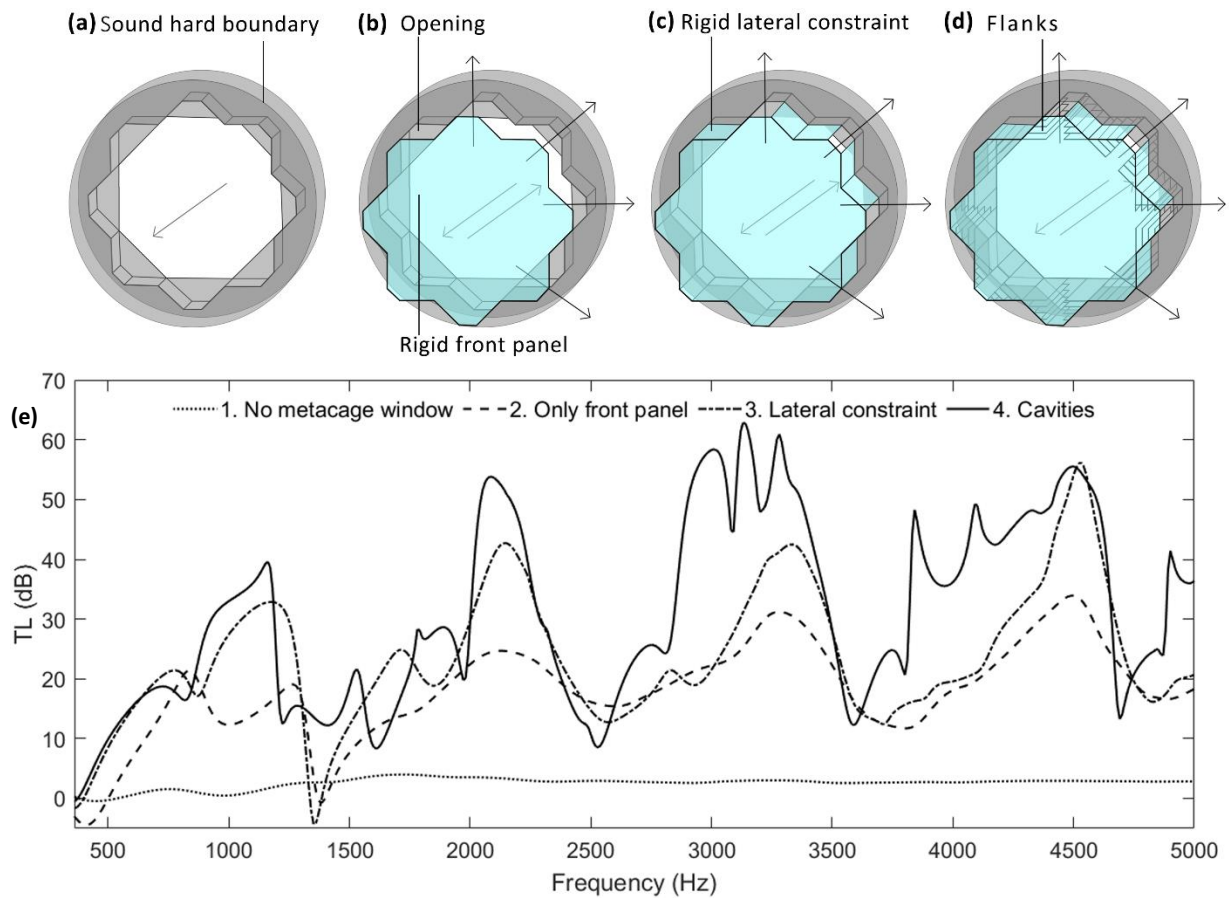
FIG. 6 Geometrical settings of 4 different internal boundary configurations: No Metacage (a), Only front panel (b), No flanks (c), Metacage (d); and Transmission Loss related to these configurations (e).

Although the front panel plays a fundamental role in noise reduction, the TL can be improved further, by adding the lateral geometrically designed constraints. Indeed, a significant TL step-up is made on the acoustic performance of the system when the lateral part is added. This particular feature differentiates the metacage window from the previous window technology attempt. [29] Thanks to their cone shape of the unit cells, their acoustical responses become exponentially divergent when they propagate in the narrowing area direction. [30]The SPL results confined in the internal geometry and within the quiet environment results much lowered (FIG. 7.b), although significant lateral SPL concentration may interfere in the metacage window performance. The final improvement of the model comes with the cavities (FIG. 6.d and FIG. 7.c), which, as proved before, at specific frequencies function as resonators. As depicted in FIG. 6.d, the TL has a much broader dome-like behaviour with this configuration with considerably higher peaks and slightly lower depths. The frequencies of effectiveness are still the same (1100, 2100, 3000, 3300, 4500 Hz) since the thickness and distance from the division is still kept the same (0.1 m). The behaviour of the slopes results slightly varying for higher values of TL probably due to simulation imprecisions, for which correction through mean value might be performed. As stated in the previous analytical analysis section, the dimension of the folded AMM period makes it more suitable for middle-high frequencies (1000 – 5000 Hz). However, if paired with the front panel and the lateral constraints, it can cover a broader frequency range even at lower frequencies (350 – 1000

Hz). As showed by FIG. 7.c, when the acoustic wave interacts with this part of the metacage window, it is drastically reduced by the destructive interference between the central duct and the lateral resonant sides of each unit cell. The overall SPL in the quiet environment results reduced and more uniformed than the previous configurations.
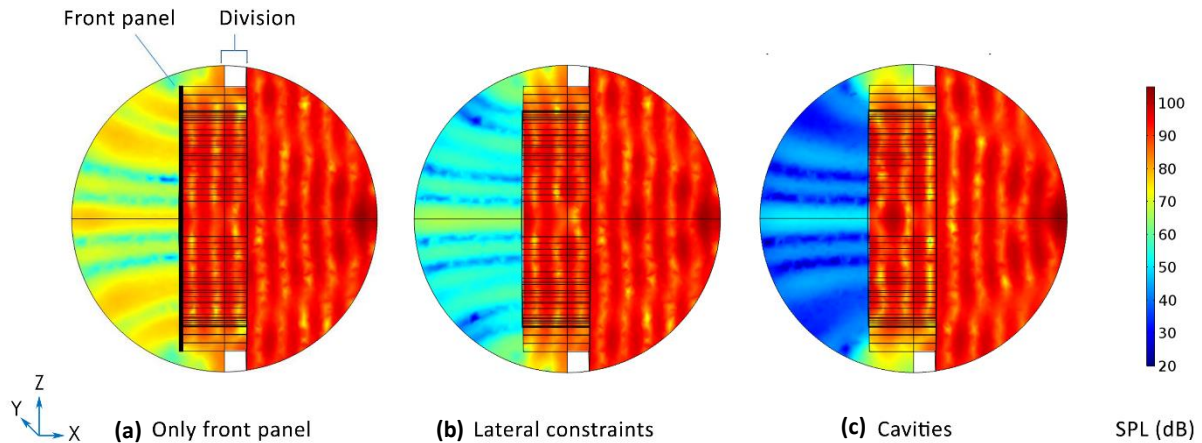

FIG. 7 SPL related to the configuration with (a) only the front panel, (b) with the front panel and the lateral constraints, and (c) with the front panel, the lateral constraints, and cavities involved in the noise reduction through the opening. The colour legend refers to dB as a measuring unit, and 3300 Hz is the analysis frequency.

5. Ventilation analysis

As mentioned in the introduction, natural ventilation is a central feature of the AMM here presented. The technique used is buoyancy, which only requests the presence of one or two openings on an external building wall, placed systematically to create a natural airflow system. In particular, buoyancy ventilation results from the difference between interior and exterior air density. This change causes the warm air to rise above the cold air, and create an upward air-stream, of which the ventilation rate can be calculated as:

$$q = AC_d\sqrt{\frac{\Delta T\, g\, h}{(T_I+273)}} \qquad \text{(m}^3\text{/s)} \qquad (3)$$

where A is the area of each opening (m²), C_d is the discharge coefficient (typically 0.6), T_I is the internal temperature (°C), ΔT is the difference between internal and external temperature (°C), g is the gravitational force (m/s²), and h is the height between openings (m). According to Bayoumi [22], (where the thermal comfort and heating and cooling energy demand are also considered) natural ventilation would occur by an opening in the building when the outdoor temperature is within ±3 °C of the indoor temperature (i.e., within +3 °C in heating; within −3 °C in cooling). So this technology is widely applicable in the majority of the environments (from a temperate climate to slightly cold or hot climate).

Besides this, Von Grabe et al. [21] investigate the matter of natural ventilation accurately in buildings through buoyancy and the flow directivity according to the window opening features. The tested window types are several: double vertical slide window, turn window, tilt window, awning window, horizontal pivot window and vertical pivot window. Different opening rates are included for each window tests to allow a more extensive comparison, and the windows performance is evaluated according to various criteria such as the mass flow and the air

change rate and the CO_2 removal rate. In their study, Van Grabe et al. highlight how the horizontal pivot window is the best performing type of window.

Due to the lateral airflow of the metacage window, this can be compared with the tilt or awning windows. In the optimisation process of combining natural ventilation with noise reduction, it was taken into account that lateral airflow such in tilt or awning windows is quite lower than the horizontal pivot window, the double vertical slide window, and turn window. These last two are meant to be better due to allowing faster air exchange since, in their design, the attenuation of outdoor inputs such as noise sources is not guaranteed. So natural ventilation is generally meant to be performed in the shortest amount of time to avoid indoor contamination with negative factors such as outdoor noise. [21] However, from the metacage window acoustic effect combined with 33% of the opening rate, a perpetual opening can be guaranteed in several outdoor noise conditions. So if we compare the effects of the horizontal tilt window on the short term with the one of the metacage window on the long term, they are equally valid.

6. Conclusions

In the presented study, a new metacage window which allows natural ventilation and noise reduction was developed through the principle of Snell's Law for AMS and investigated through semi-infinite FEM Method. The geometry was first assessed by a parametric study to determine which combination between rotation angle, cavities number and cavities width would have been the optimal one for the scope. Afterwards, four acoustic configurations were analysed to understand the impact of each part of the metacage window.

From the acoustics point of view, unit cell, AMS, and AMM have been evaluated through a sub-structural approach. Overall the metacage window design allows a TL with a minimum of 8 dB and a mean value of 30 dB within a frequency range of 350-5000 Hz. The final opening rate of the metacage window was 33%. The ventilation capacity was proved to be good enough to allow buoyancy ventilation in the conditions considered by Bayoumi[22] and the flow directivity discussed and investigated by Von Grabe et al. [21] Indoor comfort was guaranteed by the perpetual opening of the window supported by the noise reduction effect. The lateral ventilation was not the most efficient in the short term. [21] Nevertheless, in the long one, it became equally effective.

Many factors influenced the overall performance of the acoustic metacage window. Regarding the optimal combination for the structure of the unit cell, its constraints total dimension were certainly a limit in terms of noise reduction wavelength. However, in combination with the lateral metacage constraints and the front panel, they resulted in working significantly in the high frequencies (2000-4500 Hz). The unit cell array (AMS) proved to be equally efficient in the same frequency range. An additional improved performance was observed between 1000-2000 Hz. The acoustic effectiveness increased by folding the AMS into an octagonal closed shape and adding a front panel. Each part of the AMM demonstrated to give different TL contribution. The front panel gave a mean power reduction of 17.5 dB with a peak value at high frequencies. At the same time, the additional lateral constraint and the cavities increased this performance of respectively 31% and 70% with also a significant contribution at middle-low frequencies. The cavities of the unit cell played a vital role in the resonant stopband, so they improved the previously considered configuration of 30%. The TL peaks frequencies were due to the thickness of the AMM. Indeed, they were the same for all the configurations.

Further optimisation steps might clarify if this mechanism can be adapted to multiple and more conventional window's shapes and additional laboratory tests are needed to prove the effectiveness of real prototypes. However, the significant results in the acoustic part set a new AMM generation with various merits over traditional windows, including effective long term natural ventilation combined with customised noise reduction.

Acknowledgement

References

[1]   H. S. Lim and G. Kim, "The renovation of window mechanism for natural ventilation in a high-rise residential building," *Int. J. Vent.*, vol. 17, no. 1, pp. 17–30, 2018.

[2]   M. J. Sorgato, A. P. Melo, and R. Lamberts, "The effect of window opening ventilation control on residential building energy consumption," *Energy Build.*, vol. 133, pp. 1–13, 2016.

[3]   UK Space Management and Group, "UK Higher Education Space Management Project Review of space norms," 2006.

[4]   Public Health England, "Review and Update of Occupancy Factors for UK homes," 2018.

[5]   B. Lam, C. Shi, D. Shi, and W. S. Gan, "Active control of sound through full-sized open windows," *Build. Environ.*, vol. 141, pp. 16–27, 2018.

[6]   B. Lam, S. Elliott, J. Cheer, and W.-S. Gan, "Physical limits on the performance of active noise control through open windows," *Appl. Acoust.*, no. 137, pp. 9–17, 2018.

[7]   F. Asdrubali and C. Buratti, "Sound intensity investigation of the acoustics performances of high insulation ventilating windows integrated with rolling shutter boxes," *Appl. Acoust.*, vol. 66, pp. 1088–1101, 2005.

[8]   F. Cotana, A. L. Pisello, E. Moretti, and C. Buratti, "Multipurpose characterization of glazing systems with silica aerogel: In-field experimental analysis of thermal-energy, lighting and acoustic performance," *Build. Environ.*, vol. 81, pp. 92–102, 2014.

[9]   Y. G. Tong, S. K. Tang, J. Kang, A. Fung, and M. K. L. Yeung, "Full scale field study of sound transmission across plenum windows," *Appl. Acoust.*, vol. 89, pp. 244–253, 2015.

[10]   Y. Xie, W. Wang, H. Chen, A. Konneker, B. I. Popa, and S. A. Cummer, "Wavefront modulation and subwavelength diffractive acoustics with an acoustic metasurface," *Nat. Commun.*, vol. 120, no. 19, pp. 1–5, 2014.

[11]   Y. Li *et al.*, "Experimental Realization of Full Control of Reflected Waves with Subwavelength Acoustic Metasurfaces," *Phys. Rev. Appl.*, vol. 2, no. 064002, pp. 1–11, 2014.

[12]   J. Zhu *et al.*, "A holey-structured metamaterial for acoustic deep-subwavelength imaging," *Nat. Phys. Lett.*, vol. 7, pp. 52–55, 2011.

[13] S. A. Cummer *et al.*, "Scattering Theory Derivation of a 3D Acoustic Cloaking Shell," *Phys. Rev. Lett.*, vol. 100, no. 024301, pp. 1–4, 2008.

[14] C. Shen, Y. Xie, J. Li, S. A. Cummer, and Y. Jing, "Acoustic metacages for sound shielding with steady air flow," *J. Appl. Phys.*, vol. 123, p. 124501, 2018.

[15] R. Ghaffarivardavagh, J. Nikolajczyk, R. Glynn Holt, S. Anderson, and X. Zhang, "Horn-like space-coiling metamaterials toward simultaneous phase and amplitude modulation," *Nat. Commun.*, vol. 9, no. 1349, pp. 1–8, 2018.

[16] X. Yu, "Design and in-situ measurement of the acoustic performance of a metasurface ventilation window," *Appl. Acoust.*, vol. 152, pp. 127–132, 2019.

[17] X. Wang, X. Luo, B. Yang, and Z. Huang, "Ultrathin and durable open metamaterials for simultaneous ventilation and sound reduction Cite," *Appl. Phys. Lett*, vol. 115, p. 171902, 2019.

[18] H. Huang, X. Qiu, and J. Kang, "Active noise attenuation in ventilation windows," *J. Acoust. Soc. Am.*, vol. 130, p. 176, 2011.

[19] A. Selamet and Z. L. Ji, "ACOUSTIC ATTENUATION PERFORMANCE OF CIRCULAR EXPANSION CHAMBERS WITH EXTENDED INLET/OUTLET," *J. Sound Vib.*, vol. 223, no. 2, pp. 197–212, 1999.

[20] N. Sellen, M. Cuesta, and M.-A. Galland, "Noise reduction in a flow duct: Implementation of a hybrid passive/active solution," *J. Sound Vib.*, vol. 297, pp. 492–511, 2006.

[21] J. Von Grabe, P. Svoboda, and A. Bäumler, "Window ventilation efficiency in the case of buoyancy ventilation," *Energy Build.*, vol. 72, pp. 203–211, Apr. 2014.

[22] M. Bayoumi, "Impacts of window opening grade on improving the energy efficiency of a façade in hot climates," *Build. Environ.*, vol. 119, pp. 31–43, 2017.

[23] X. Yu, Z. Lu, L. Cheng, and F. Cui, "On the sound insulation of acoustic metasurface using a sub-structuring approach," *J. Sound Vib.*, vol. 401, pp. 190–203, 2017.

[24] K. J. B. Lee, M. K. Jung, and S. H. Lee, "Highly tunable acoustic metamaterials based on a resonant tubular array," *Phys. Rev. B*, vol. 86, p. 184302, 2012.

[25] O. Guasch, M. Arnela, and P. Sánchez-Martín, "Transfer matrices to characterize linear and quadratic acoustic black holes in duct terminations," *J. Sound Vib.*, vol. 395, pp. 65–79, 2017.

[26] J. Woong Jung, J. Eun Kim, and J. Woo Lee, "Acoustic metamaterial panel for both fluid passage and broadband soundproofing in the audible frequency range," *Appl. Phys. Lett*, vol. 112, p. 41903, 2018.

[27] N. Yu *et al.*, "Flat optics: Controlling wavefronts with optical antenna metasurfaces," *IEEE J. Sel. Top. Quantum Electron.*, vol. 19, no. 3, p. 4700423, 2013.

[28] E. Qian, Y. Fu, Y. Fu, and H. Chen, "Total omnidirectional reflection by sub-wavelength gradient metallic gratings ," *epl J.*, no. 114, p. 34003, 2016.

[29] M. H. F. De Salis, D. J. Oldham, and S. Sharples, "Noise control strategies for naturally ventilated buildings," *Build. Environ.*, vol. 37, pp. 471–484, 2000.

[30] A. Barjau, "On the one-dimensional acoustic propagation in conical ducts with stationary mean flow," *Cit. J. Acoust. Soc. Am.*, vol. 122, p. 3242, 2007.